Calcium Block of Single Sodium Channels: Role of a Pore-Lining Aromatic Residue

Vincent P. Santarelli,* Amy L. Eastwood,† Dennis A. Dougherty,† Christopher A. Ahern,* and Richard Horn*
*Department of Molecular Physiology and Biophysics, Institute of Hyperexcitability, Jefferson Medical College, Philadelphia, Pennsylvania; and †Division of Chemistry and Chemical Engineering, California Institute of Technology, Pasadena, California

ABSTRACT Extracellular Ca^{2+} ions cause a rapid block of voltage-gated sodium channels, manifest as an apparent reduction of the amplitude of single-channel currents. We examined the influence of residue Tyr-401 in the isoform $rNa_V1.4$ on both single-channel conductance and Ca^{2+} block. An aromatic residue at this position in the outer mouth of the pore plays a critical role in high-affinity block by the guanidinium toxin tetrodotoxin, primarily due to an electrostatic attraction between the cationic blocker and the system of π electrons on the aromatic face. We tested whether a similar attraction between small metal cations (Na^+ and Ca^{2+}) and this residue would enhance single-channel conductance or pore block, using a series of fluorinated derivatives of phenylalanine at this position. Our results show a monotonic decrease in Ca^{2+} block as the aromatic ring is increasingly fluorinated, a result in accord with a cation-π interaction between Ca^{2+} and the aromatic ring. This occurred without a change of single-channel conductance, consistent with a greater electrostatic effect of the π system on divalent than on monovalent cations. High-level quantum mechanical calculations show that Ca^{2+} ions likely do not bind directly to the aromatic ring because of the substantial energetic penalty of dehydrating a Ca^{2+} ion. However, the complex of a Ca^{2+} ion with its inner hydration shell, $Ca^{2+}(H_2O)_6$, interacts electrostatically with the aromatic ring in a way that affects the local concentration of Ca^{2+} ions in the extracellular vestibule.

INTRODUCTION

Voltage-gated sodium channels are transmembrane proteins involved critically in a variety of physiological functions, including muscle contraction, generation of action potentials in neurons, and secretion of neurotransmitters and hormones. These channels control the diffusion of Na^+ ions across the cell membrane in response to changes of transmembrane potential. When open, ion channels allow high ionic fluxes while discriminating among ions based on charge and size. Understanding the basis of Na^+ permeation requires the identification of amino acids that form the selectivity filter, a narrow region of the pore where ions are partially dehydrated. As in structurally similar potassium and calcium channels, sodium channels have a pore or ''P'' region, a reentrant loop between the fifth and sixth transmembrane spanning segments in each of four homologous domains (Fig. 1). This P region houses the selectivity filter. In sodium channels, there are four key residues responsible for determining the selectivity of Na^+ over other cations (Fig. 1, *boxed residues*). These residues, one from each domain (D), are Asp (D1), Glu (D2), Lys (D3), and Ala (D4), referred to as DEKA (1). Mutation of any of these residues alters the channel's selectivity.

The side chain of Lys (D3) is perhaps the most important player of DEKA. Changing from DEKA to DEAA eliminates selectivity among monovalent cations (Li^+, Na^+, K^+, Rb^+, and Cs^+) and enhances permeability to divalent cations (Mg^{2+}, Ca^{2+}, and Ba^{2+}) (1–5). Enhanced Ca^{2+} permeation is obtained for all charge-altering substitutions of Lys (D3), but not by substitution with a charge-preserving Arg (2). By contrast, wild-type (WT) sodium channels are typically blocked by extracellular Ca^{2+} ions. The apparent blocking affinity is strongly correlated with the overall negative charge of residues at the DEKA positions, establishing an important role of electrostatics (3). The close relationship between selectivity and block in these studies suggests that external Ca^{2+} block occurs at or near the DEKA ring (5).

Single-channel measurements have shown that block by extracellular Ca^{2+} is voltage-dependent and fast, manifest as an apparent reduction of single-channel current amplitude. Estimates of the inhibition constant range between 10 and 35 mM, with the blocking site apparently located 20–30% of the way into the transmembrane electric field (3,6–11). A separate effect of changing external Ca^{2+} concentration ($[Ca^{2+}]$) is a shift in the activation gating range for sodium channels. This phenomenon has been ascribed to Ca^{2+} ions screening and/or binding to negative surface charges that influence the voltage-sensing mechanism (12).

Charge-altering mutations involving either DEKA or a more extracellular ring of negatively charged residues (Fig. 1, *underlined residues EEDD*) strongly reduce block by the guanidinium toxins tetrodotoxin (TTX) and saxitoxin. Mutations of residues adjacent to these two charged rings typically have smaller effects, if any, on toxin block. These experiments suggest that the charged rings create part of the extracellular mouth or pore wall of the sodium channel (13). In addition, neutralizing any negative residue causes a decrease in single-channel conductance, consistent with the idea that the negative charges act to concentrate cations in

Submitted February 20, 2007, and accepted for publication May 22, 2007.

Address reprint requests to Dr. Richard Horn, Division of Chemistry and Chemical Engineering, California Institute of Technology, Pasadena, CA 91125. Tel.: 215-503-6725; Fax: 215-503-2073; E-mail: Richard.Horn@jefferson.edu.

Editor: Dorothy A. Hanck.

0006-3495/07/10/2341/09 $2.00

doi: 10.1529/biophysj.107.106856

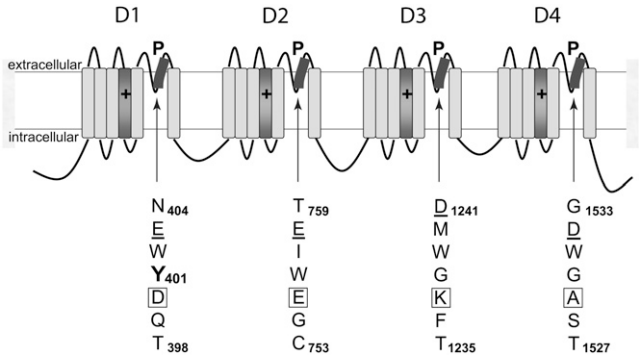

FIGURE 1 Topology of a voltage-gated sodium channel. Sodium channels are comprised of 4 domains (D1–D4), each with six transmembrane segments (S1–S6). S4 is the primary component of the voltage-sensor (+), and the loop between S5-S6 is the pore (*P*) region. The aa sequence of the highlighted portion of the pore is shown below each domain. The DEKA ring is outlined, the outer negative ring underlined. Y401 in D1 is one residue above the DEKA ring.

the extracellular vestibule of the pore (13). Nevertheless, the influence of charged vestibule residues on Na^+ permeation cannot be explained entirely by the charges of these residues (2,14,15).

Charged residues are not the only determinants of permeation and pore block. An aromatic residue in D1, either Tyr or Phe, is found exclusively in sodium channels that have nanomolar affinity for TTX block (16–20). This residue, Tyr-401 in $rNa_V1.4$, is located between the charged rings in the primary sequence (Fig. 1). Mutating this residue to Cys, its homolog in the TTX-resistant cardiac channel $Na_V1.5$, results in a decrease in TTX sensitivity, as well as in single-channel conductance (16,17). The lowered conductance is similar in magnitude to that found in $hNa_V1.5$ (16,17). Interestingly, the converse mutation in $hNa_V1.5$ (C374Y) produces no change in single-channel conductance (17). This residue also affects Ca^{2+} block. Single-channel recording shows that $Na_V1.4$ is more sensitive to Ca^{2+} block than $Na_V1.5$ (21,22); however, see (10,11). This observation leads naturally to the question of how a hydrophobic aromatic residue could enhance the pore block of a small metal cation. One possibility is an electrostatic attraction between the π electrons of the aromatic ring and the cationic blocker.

Recently, we investigated the role of a cation-π interaction between TTX and the aromatic face of Tyr-401 in $rNa_V1.4$ (23). This study used in vivo nonsense suppression to incorporate unnatural amino acid analogs of Phe at position 401. Our results showed a monotonic decrease in TTX block as the aromatic ring was increasingly fluorinated, a manipulation that reduces the negative electrostatic potential on the aromatic face. We hypothesize that this negative potential would attract cations that either permeate or block the channel. Our intention here is not to explore the isoform differences that might affect permeation or Ca^{2+} block. Rather we focus on residue 401 of $rNa_V1.4$ and ask 1), whether a cation-π interaction is a contributing factor, based on experimental data; and 2), whether such an interaction between a metal cation and an aromatic ring can be rationalized theoretically in an aqueous environment.

MATERIALS AND METHODS

Molecular biology and unnatural amino acids

The channel used, pBSTA/$rNa_V1.4$, was a gift from Drs. Baron Chanda and Francisco Bezanilla. The in vivo nonsense suppression methodology was performed as described previously (24,25). Tyr-401 of $Na_V1.4$ cDNA was mutated into a TAG (Amber stop codon) by standard mutagenesis (QuickChange, Stratagene, La Jolla, CA) and complementary mRNA was transcribed from this mutated cDNA (mMessage mMachine, Ambion, Austin, TX). Unnatural amino acids (aa) were coupled to the dinucleotide dCA, protected with nitroveratryloxycarboyl (NVOC), activated as the cyanomethyl ester, and then ligated to a modified tRNA from *Tetrahymena thermophila*. This tRNA contains a complementary anticodon to the UAG stop site in the $Na_V1.4$-Y401TAG cRNA. Deprotection of the aminoacylated tRNA-aa was performed by UV irradiation immediately before injection into Stage V-VI *Xenopus* oocytes. Typically, 20 ng of tRNA-aa, 25 ng of $Na_V1.4$-401TAG cRNA, and 2 ng of sodium channel β_1 subunit cRNA (26) were coinjected in a 50-nl volume into each oocyte.

In this study, we used Phe amino acid derivatives appended with fluorines, termed $4F_1$-Phe (single fluorination at position 4), $3,5F_2$-Phe (fluorination at the 3 and 5 positions), and $3,4,5F_3$-Phe (fluorination at the 3, 4, and 5 positions), where Cγ is position 1 on the aromatic ring.

Electrophysiology and analysis

Single-channel currents were recorded in the outside-out configuration from *Xenopus* oocytes using an Axopatch 200B amplifier (Molecular Devices, Sunnyvale, CA), 1–4 days after RNA injection. Patches were obtained in 2 mM Ca^{2+} external solution and the bath was exchanged to solutions with different [Ca^{2+}], as needed, using an ALA BPS-4 perfusion system (ALA Scientific, Westburg, NY). Pipette resistance ranged from 0.9 to 2.0 MΩ. The external solution consisted of (in mM) 150 NaCl, 2 KCl, (either 0, 0.1, 2, or 10) $CaCl_2$, 1 $MgCl_2$, and 10 HEPES, pH 7.4; and the internal solution 130 CsF, 10 CsCl, 5 EGTA, and 10 Cs-HEPES, pH 7.3. Corrections were made for liquid junction potentials. Data were low-pass filtered at 5 kHz upon acquisition, and further filtered at 4 kHz offline for analysis of single-channel amplitudes. Fenvalerate (Sigma-Aldrich, St. Louis, MO) was added to the internal solution at 10–20 μM to produce prolonged open times and enhance open probability at more hyperpolarized voltages (27). The voltage protocol consisted of a holding potential between -100 and -120 mV and 30-ms test pulses to activate the channels. In some patches, we measured single-channel currents during deactivating tail currents to -70 or -80 mV after a depolarized activating pulse. Amplitudes of single-channel openings were estimated either from amplitude histograms or by cursors in Clampfit (Molecular Devices).

Electrostatic potentials and electrostatic interactions between benzene and a Ca^{2+} ion were calculated by high-level ab initio methods using the program Jaguar (http://www.schrodinger.com/). The Ca^{2+}-benzene complex was optimized in the gas phase using the Hartree-Fock model with the split valence 6-31++G** basis set. We computed the free energy of Ca^{2+} interaction with a benzene ring at the same level of theory, accounting both for the gas-phase ab initio energies and the energies of hydration, using a self-consistent reaction field method with the Poisson-Boltzmann (P-B) solver in Jaguar (28). No corrections were made for basis set superposition error. The free energy of interaction for each geometry considered was calculated, by a standard thermodynamic cycle, as

$$\text{Interaction energy} = E_{\text{Ca}-\text{Benz}_j(\text{gas})} - E_{\text{Ca(gas)}} - E_{\text{Benz}_j(\text{gas})} + \Delta G_{\text{Ca}-\text{Benz}_j(\text{hyd})} - \Delta G_{\text{Ca(hyd)}} - \Delta G_{\text{Benz}_j(\text{hyd})},$$

where j represents the number of fluorines on the benzene ring, $E_{\text{Ca-Benz}_j\text{(gas)}}$ is the gas-phase energy of the complex, $E_{\text{Ca(gas)}}$ and $E_{\text{Benz}_j\text{(gas)}}$ are gas-phase energies of either a Ca^{2+} ion or benzene, and the free energies of hydration are similarly defined as $\Delta G_{\text{Ca-Benz}_j\text{(hyd)}}$, $\Delta G_{\text{Ca(hyd)}}$, and $\Delta G_{\text{Benz}_j\text{(hyd)}}$. The P-B solver was also used, at the same level of theory, to estimate the electrostatic potential projecting along the C_6 axis from the center of a fluorinated benzene ring in aqueous solution.

The coordinates of a Ca^{2+} ion with its first hydration shell, $Ca^{2+}(H_2O)_6$, were optimized at the DFT(B3LYP)/6-31++G** level in the gas phase. The coordinates of this optimized structure were frozen while optimizing its interaction with benzene in the gas phase at the HF/6-31++G** level, and the interaction energies between calcium hexahydrate and benzene were calculated at this optimized geometry, as above. The energy of a Na^+ ion binding at the optimized location for a Ca^{2+} ion (see Fig. 6 *C*) was determined at the HF/6-31++G** level in an aqueous environment.

RESULTS

Outside-out patches from oocytes were used to measure single-channel Na^+ currents. Fig. 2 *A* shows representative single-channel currents of the mutant Y401F ($rNa_V1.4$ normally has a Tyr at this position) in response to a depolarization to −50 mV (*arrow*), using an extracellular solution containing 2 mM Ca^{2+}. This mutant was created by standard mutagenesis and serves as our control for unnatural aa substitutions. The data in Fig. 2 *A* were converted to an amplitude histogram that was fit by a sum of two Gaussian functions (Fig. 2 *B*). Notice the slight excess of points between the two prominent peaks, largely a consequence of a single opening at a subconductance level. The mean current level was estimated as the difference between the means of each Gaussian function, −1.9 pA at this membrane potential. The prolonged open durations in our experiments are a consequence of internal modification by fenvalerate, which does not affect the single-channel conductance (27). In agreement with this, Fig. 2 *C* shows indistinguishable amplitudes of single-channel currents of WT $rNa_V1.4$ recorded without (*open circles*) and with (*triangles*) 20 μM fenvalerate added to the pipette, in this case in the absence of added Ca^{2+}.

Fig. 3 shows representative single-channel openings at −60 mV, in either 0.1 (below) or 10 mM external Ca^{2+} (above). Raising the external [Ca^{2+}] reduces the amplitude of single Phe-401 channel currents (Fig. 3 *A*) due to Ca^{2+} block (3,6,8–10,21,22). Fig. 3 *B* shows that Ca^{2+} also blocks the trifluorinated mutant $3,4,5F_3$-Phe401, although less effectively (*arrow*/*dashed line* shows current amplitude for the Y401F mutant in Fig. 3 *A*). Trifluorination approximately abolishes the negative electrostatic potential of an aromatic ring (29,30) without significantly affecting hydrophobicity, polarizability, or shape, suggesting that the change in electrostatics is responsible for the relief of Ca^{2+} block in this experiment. Insets show color-coded electrostatic potential surfaces of benzene and the trifluorinated derivative. On this color scale, red, blue, and green indicate negative, positive, and zero electrostatic potential, respectively. In contrast to the effect on Ca^{2+} block, the single-channel conductance in 0.1 mM extracellular Ca^{2+} was not significantly

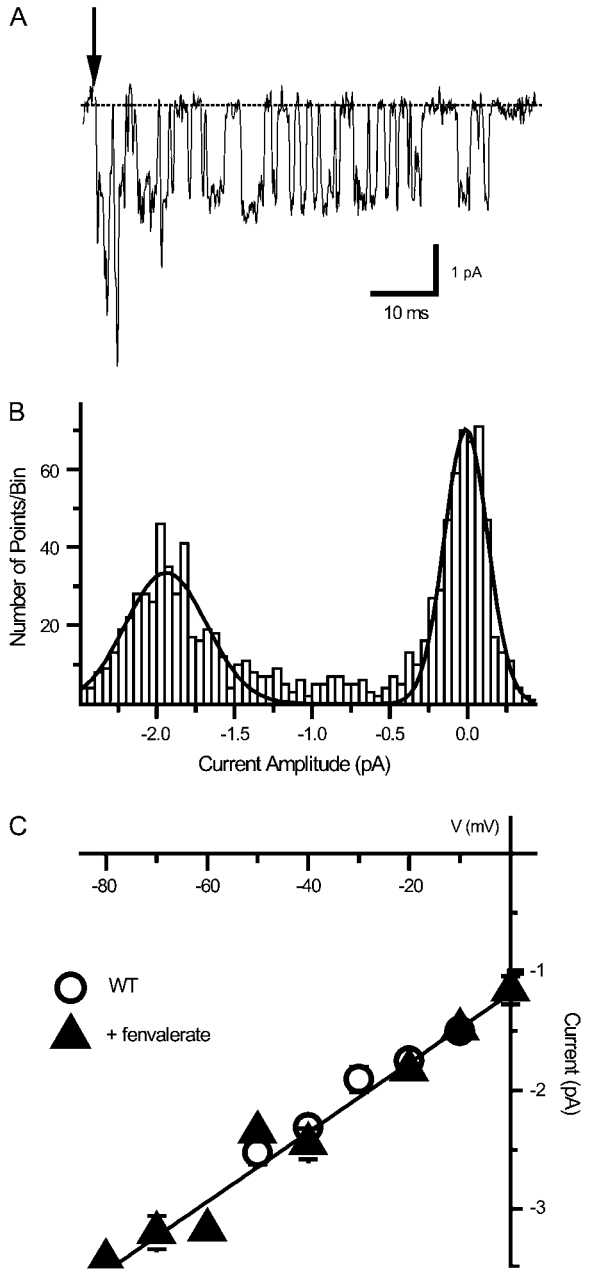

FIGURE 2 Representative single-channel recording, histogram analysis, and current-voltage relationship. (*A*) Single-channel currents of Y401F, with 2 mM Ca^{2+}, in response to a 30-ms depolarization (*arrow*) to −50 mV. Prolonged open durations are due to the effects of 10 μM intracellular fenvalerate. (*B*) Data from *A* converted to an amplitude histogram and fit by a sum of two Gaussian functions. The single-channel current amplitude is −1.9 pA at this membrane potential. (*C*) Single-channel amplitude versus voltage of wild-type $rNa_V1.4$ recorded without (*open circles*) and with (*triangles*) 10 μM internal fenvalerate; 0 mM Ca^{2+}. Data from two to five patches at each membrane potential. Fenvalerate shifts the activation range in the hyperpolarizing direction but does not change the single-channel current amplitude. The regression line was from the fit to the data for fenvalerate.

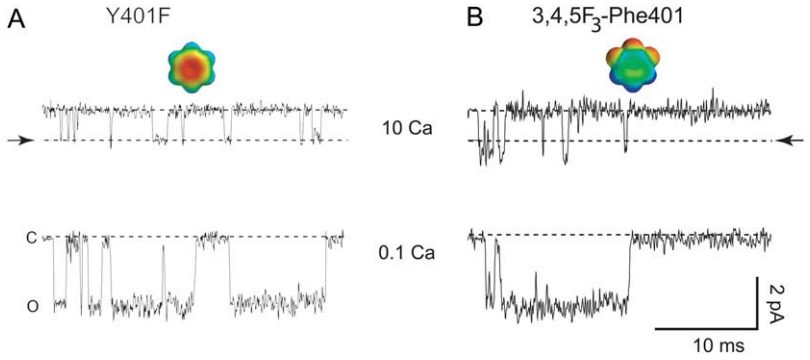

FIGURE 3 Fluorination of Phe-401 reduces sensitivity of the channel to Ca^{2+} block. Single-channel currents in response to a depolarization to −60 mV in either 10 or 0.1 mM external Ca^{2+}. Openings are downward. (*A*) Single-channel recordings of the mutant Y401F. Raising the external $[Ca^{2+}]$ from 0.1 mM to 10 mM Ca^{2+} reduces the amplitude of the single-channel current. (*B*) Currents of the mutant 3,4,5F_3-Phe. The two channel constructs have similar current amplitudes in 0.1 mM Ca^{2+}. However, fluorination of Phe-401 relieves Ca^{2+} block. Arrow shows the current amplitude of Y401F in 10 mM Ca^{2+} (mean of four patches). Insets show color-coded electrostatic surfaces of benzene and 3,4,5F_3-benzene (*blue*, +20 kcal/mol; *red*, −20 kcal/mol).

different among the fluorinated variants of Phe-401, ranging between 23.2 ± 2.2 pS for 4F_1-Phe401 and 25.9 ± 1.6 pS for 3,5F_2-Phe401 (Fig. 4, *legend*). This result is consistent with a greater effect of the negative electrostatic potential on the local concentration of Ca^{2+} ions than on that of Na^+ ions at the entrance of the selectivity filter.

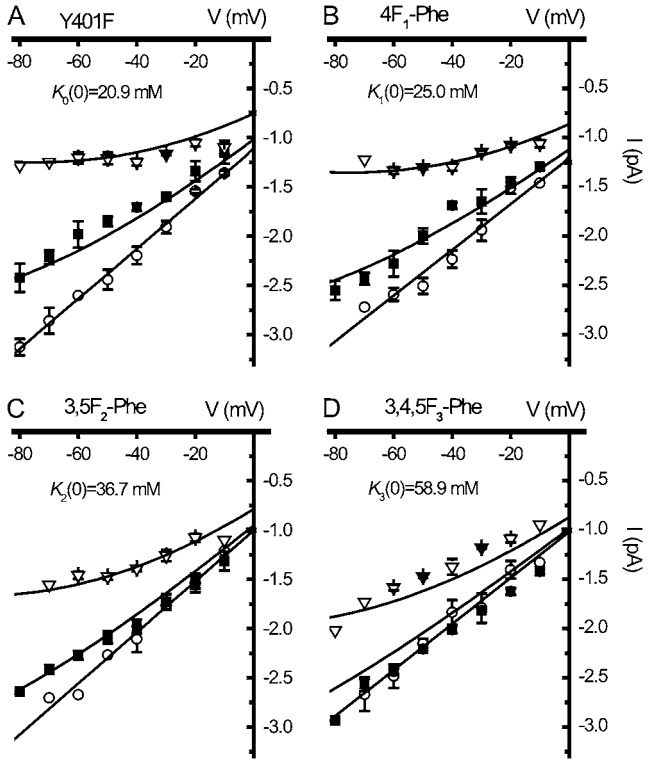

FIGURE 4 Single-channel current-voltage relationships of Phe-401 mutants. Ca^{2+} concentrations are 0.1 mM (*open circles*), 2 mM (*solid squares*), and 10 mM Ca^{2+} (*open triangles*). Each symbol represents data from two to eight patches. Data for 0.1 mM Ca^{2+} were fit by straight lines (slopes: 25.3 ± 0.8, 23.2 ± 2.2, 25.9 ± 1.6, and 23.4 ± 1.6 pS, for Y401F, 4F_1-Phe, 3,5F_2-Phe, and 3,4,5F_3-Phe, respectively), whereas fractional block at higher $[Ca^{2+}]$ was fit by a Woodhull model (see Results). The curvature of the current-voltage relationship illustrates the voltage-dependent block. The effective fraction through the electric field (δ) for Ca^{2+} block, constrained to be the same for each Phe variant, was 0.18 ± 0.03. Note the decrease in Ca^{2+} block with increased fluorination. The estimates of inhibition constants were $K_0(0) = 20.9 \pm 2.8$ mM, $K_1(0) = 25.0 \pm 3.2$ mM, $K_2(0) = 36.7 \pm 5.1$ mM, and $K_3(0) = 58.9 \pm 9.2$ mM.

Single-channel current-voltage relationships for Phe-401 and three fluorinated mutants are shown in Fig. 4 at three different Ca^{2+} concentrations, 0.1 mM (*open circles*), 2 mM (*solid squares*), and 10 mM (*open triangles*). Because the patches tended to be unstable in the absence of added Ca^{2+}, and because the amplitudes of single-channel currents were indistinguishable between 0 and 0.1 mM Ca^{2+} (data not shown), we used 0.1 mM Ca^{2+} as the unblocked control. The single-channel current-voltage relationships in 0.1 mM extracellular Ca^{2+} were fit by straight lines, and the fractional block at higher $[Ca^{2+}]$ is represented as

$$\frac{I([Ca^{2+}],V)}{I([Ca^{2+}]=0.1\,\mathrm{mM},V)}=\frac{K(V)}{K(V)+[Ca^{2+}]}.$$

The voltage-dependent inhibition constant $K(V)$, based on a simple Woodhull-type model (31), is defined as

$$K(V)=K_j(0)\exp\left(\frac{\delta zFV}{RT}\right),$$

where V is the membrane potential, $K_j(0)$ is the inhibition constant at 0 mV for a mutant containing j fluorines ($j = 0$, 1, 2, 3) at Phe-401, δ is the effective fraction through the electric field for a blocker with valence z, and $RT/F = 25$ mV at room temperature. For the least-squares fit, the value of δ was constrained to be identical for all Phe-401 mutants. The monotonic effect of fluorination on Ca^{2+} block is evident from the block observed at 2 mM Ca^{2+} and from the estimated values of $K_j(0)$ (Fig. 4, *legend*, and Fig. 5). The curvature of the current-voltage relationship, most obvious at 10 mM Ca^{2+}, is indicative of the voltage dependence of the block. The estimated value of δ was 0.18 ± 0.03, comparable to previous estimates for Ca^{2+} block of single sodium channels (6,10,11). The curvature of the current-voltage relationship is noticeably muted in the trifluorinated mutant (Fig. 4 *D*). Although we can only speculate on this observation, it suggests either that the blocking site is more superficial in this mutant, or that trifluorination reduces the local concentration of cations (see Discussion) whose distribution might be affected by membrane potential.

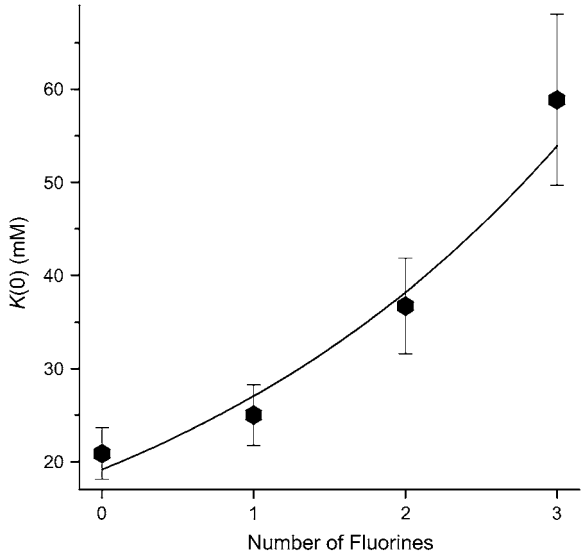

FIGURE 5 Exponential effect of fluorination on the inhibition constant for Ca^{2+} block. The data points are the estimates (± standard error) of the inhibition constants at 0 mV, i.e., $K_j(0)$, from Fig. 4 (j is the number of fluorines). The best-fit theoretical curve is $K_j(0) = 19.2\exp(0.344j)$ mM.

DISCUSSION

The side chains of amino acids that line the extracellular aqueous vestibule of a sodium-channel pore could affect permeation in a variety of ways, primarily by consequences on the local concentration or hydration of permeant ions and blockers. Amino acid side chains may, for example, interact directly (i.e., within the range of van der Waals forces) with ions in the vestibule. For permeant ions, such contacts would generally have to be brief to be consistent with the high transport rate through open channels. Vestibule-lining side chains could also contribute to the electrostatic potential experienced by ions. Finally, the protein lining of the vestibule effectively decreases the local dielectric constant compared to water by presenting a dielectric boundary (32,33). Deeper residues that line the selectivity filter presumably have the most intimate contact with permeant ions, and also perhaps with small pore blockers. Large effects on permeation and/or block in sodium channels are caused by mutations of either the DEKA selectivity ring or the outer EEDD ring of negative charges (1–5,13,14,19,34–37). The main exception to these generalities involves the aromatic residue Tyr-401 in $rNa_V1.4$ and aligned residues in other isoforms. A neutral, nonaromatic substitution of this residue decreases TTX affinity by as much as three orders of magnitude (16–18). A substantial component of cationic TTX's binding energy is due to an electrostatic interaction with the π system of Tyr-401 (23), suggesting that the aromatic ring is oriented to face the permeation pathway. This raises the possibility that other extracellular cations, especially Na^+ and Ca^{2+}, are also attracted to the negative electrostatic potential on the aromatic face of this residue.

The electrostatic potential projecting out from the center of a benzene ring in aqueous solution, and the effects on it of fluorination, are shown in Fig. 6 *A*. These estimates agree with experimental and theoretical analyses showing that trifluorination effectively neutralizes the quadrupole moment (29,30). In fact, the quadrupole moment is slightly reversed in sign by trifluorination (Fig. 6 *A*), in agreement with experimental observations (38). The results of this study show that systematic fluorination of the aromatic ring progressively reduces Ca^{2+} block without affecting the single-channel conductance for Na^+ ions. We explore here whether these results are consistent with an electrostatic mechanism.

A negative electrostatic potential on the aromatic face of residue 401 could enhance Ca^{2+} block in two ways. First, a Ca^{2+} ion might bind directly (essentially at van der Waals contact) to the face of the aromatic ring where it would prevent the flux of Na^+ ions. Second, the negative potential might increase the probability that a Ca^{2+} ion would be found in the vicinity of the blocking site without direct contact between the metal ion and the aromatic ring. We favor the second scenario. Direct binding of Ca^{2+} to a simple aromatic ring would require partial dehydration of the Ca^{2+} ion, an energetically costly task for the diffuse quadrupole moment of an aromatic ring (39). To show this explicitly, we determined the binding energy of a Ca^{2+} ion to benzene, using high-level (HF/6-31++G**) ab initio calculations. The optimized position for Ca^{2+} in the gas phase was on the C_6 symmetry axis of the benzene ring 2.54 Å from its center (Fig. 6 *B*). Although the interaction energy is highly favorable at this position in the gas phase, −64 kcal/mol, the Gibbs free energy for Ca^{2+} binding in an aqueous environment is highly unfavorable, +31 kcal/mol, a consequence of the substantial mismatch between the hydration energies of a Ca^{2+} ion ($\Delta G_{Ca(hyd)} = -390$ kcal/mol) and benzene ($\Delta G_{Benz(hyd)} = -1.5$ kcal/mol). We present this result graphically in Fig. 6 *B* by plotting the calculated free energy of the interaction of a Ca^{2+} ion with benzene as a function of distance from the center of the benzene ring. The solid and dotted lines represent the interaction energy in the gas phase and in aqueous solution, respectively. Benzene (*black*) attracts a Ca^{2+} ion in the gas phase and repels it in water; this conclusion holds at any distance $>\sim 2$ Å from the center of the aromatic ring.

Fig. 6 *B* also shows the effect of fluorination on these interaction energies. The vertical dotted line highlights these energies at the optimized position of Ca^{2+} in the gas phase. Both in gas and in aqueous solution, fluorination diminishes the energy of interaction between Ca^{2+} and benzene at distances closer than ~4.5 Å. Note that at larger distances water molecules would be able to penetrate the space between the cation and the aromatic ring. Therefore, although a benzene ring has a net repulsive effect on a Ca^{2+} ion in water, the repulsion is exacerbated by fluorinating the ring. From the point of view of a cation, we might say that the negative electrostatic potential ameliorates the hydrophobic (unattractive) properties of the aromatic side-chain. These calculations

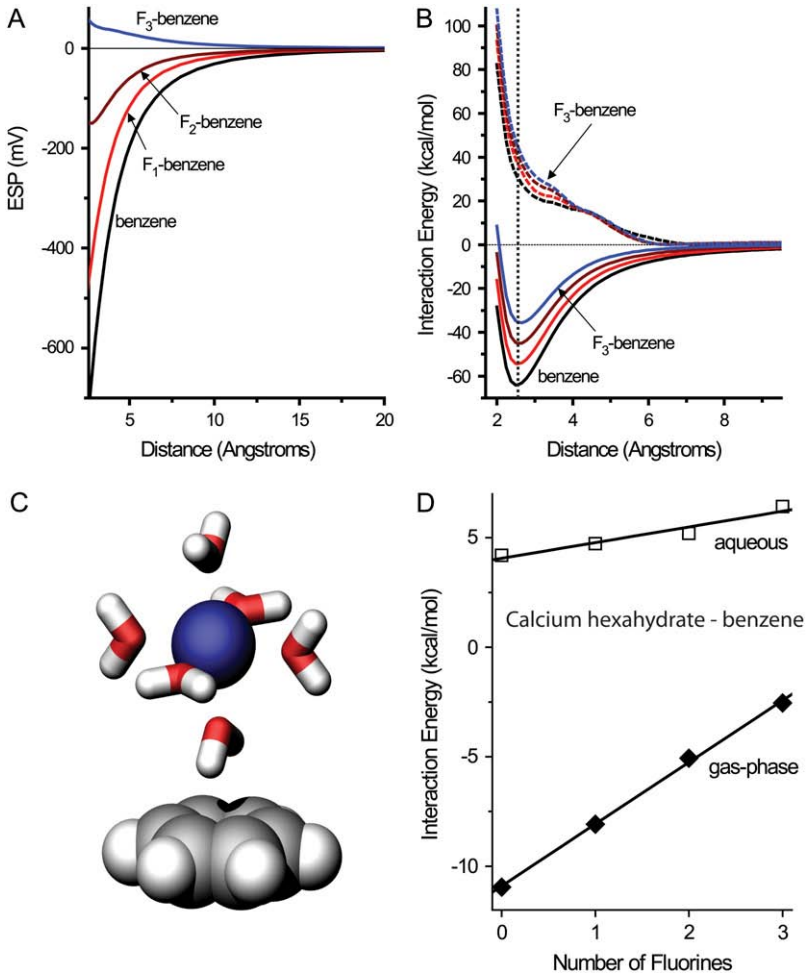

FIGURE 6 Electrostatic potentials and Ca^{2+}-binding energies. (*A*) Electrostatic potential (*ESP*) for benzene and its fluorinated derivatives. Electrostatic potential was determined along the C_6 axis projecting from the center of the benzene ring using a polarizable continuum model of water. (*B*) Interaction energy of a Ca^{2+} ion with benzene and fluorinated derivatives along the C_6 axis. Gas-phase energies are plotted as solid lines, and aqueous energies as dashed lines. Values were calculated in 0.5-Å increments from 2 to 4 Å and in 1-Å increments for greater distances. The vertical dotted line is set at the minimum-energy distance between the Ca^{2+} ion and benzene. This line shows that progressive fluorination monotonically destabilizes the attraction of Ca^{2+} for the aromatic ring. (*C*) Optimized geometry of the complex between calcium hexahydrate and a benzene ring. (*D*) Interaction energy between calcium hexahydrate and benzene, calculated in gas or in water at the optimized geometry shown in *C*. The energies increase linearly with the number of added fluorines.

strongly suggest that in aqueous solution Ca^{2+} ions do not make direct contact with the aromatic ring of Tyr-401 (or Phe-401), but that fluorination nevertheless has an electrostatic effect on Ca^{2+} ions in the vicinity of the ring. To rationalize the unfavorable interaction energies in water, we explore an alternative viewpoint, namely, that an appropriate treatment of the interaction between an aromatic ring and Ca^{2+} must include explicit water, specifically the inner hydration shell of the cation.

The substantial desolvation penalty for a Ca^{2+} ion, ~30 kcal/mol to remove one water molecule from the inner hydration shell, indicates that when interacting with an aromatic ring, Ca^{2+} will maintain this hydration shell of six waters (40,41). Nevertheless, the charge of the cation will orient and polarize the hydration waters so that the hydrated complex, $Ca^{2+}(H_2O)_6$, can interact favorably with the face of an aromatic ring (42,43). In essence, calcium hexahydrate is a larger, more polarizable cation than an isolated Ca^{2+} ion. The increased size and delocalized charge is expected to decrease the interaction energy with a benzene ring (43–45). Fig. 6 *C* shows the octahedral arrangement of waters in calcium hexahydrate and the optimized geometry of this metal-water complex with benzene. The Ca^{2+} ion lies 5.70 Å from the centroid of benzene at an angle of 8.9° from the normal of the aromatic ring plane. The interaction energies of calcium hexahydrate with benzene in this optimized geometry are −10.6 and +3.7 kcal/mol in gas and water, respectively, significantly smaller in magnitude than the energies observed for an isolated Ca^{2+} ion, in part because of the greater distance between hydrated calcium and the benzene ring. We determined the effect of fluorinating the benzene ring on the binding energy of calcium hexahydrate, calculated at the fixed, optimized geometry shown in Fig. 6 *C*. These interaction energies are plotted in Fig. 6 *D* as a function of the number of fluorine atoms appended to the benzene ring. As in the case of a nonhydrated Ca^{2+} ion (Fig. 6 *B*, *vertical dotted line*), the interaction energy increases monotonically as the benzene ring is progressively fluorinated (Fig. 6 *D*). The relationship is steeper when calculated in the gas phase.

The energetic effect of altering the benzene ring, a linear increase in interaction energy with fluorination (Fig. 6 *D*), leads to a prediction of the consequences of fluorination on Ca^{2+} block. Fig. 7 shows a molecular model of the outer vestibule of the pore of the sodium channel (46), with calcium hexahydrate aligned in its optimized geometry with

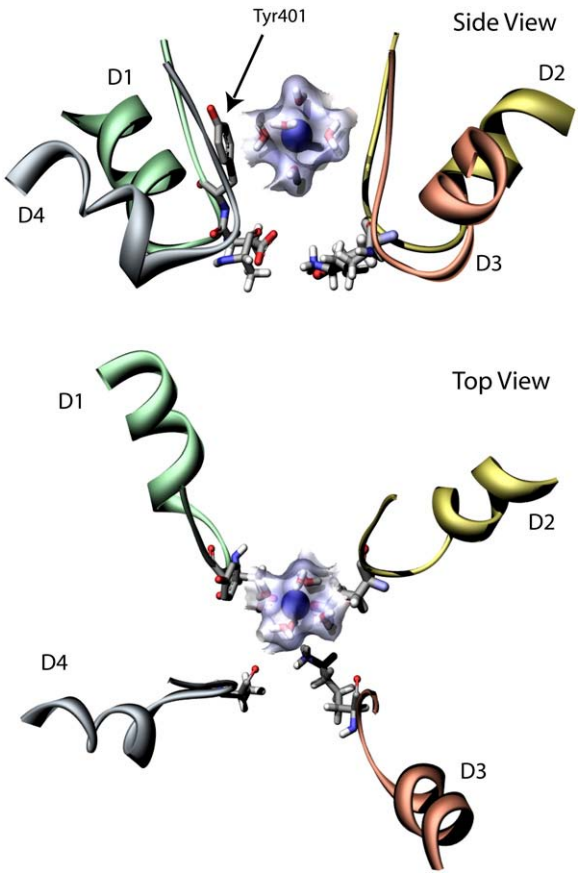

FIGURE 7 Model of the extracellular vestibule of the channel showing calcium hexahydrate in optimal apposition to Tyr-401 (Fig. 6 *C*). The molecular model (46) depicts part of the pore helix and pore loop from each domain of the sodium channel. The side chains of Tyr-401 and the DEKA ring are rendered. Calcium hexahydrate is shown enveloped by a transparent solvent-accessible surface.

the aromatic ring of Tyr-401. The side chains of the DEKA ring are shown below Tyr-401. The transparent, solvent-accessible surface of the hydrated Ca^{2+} ion is also shown. Previous modeling and experimental evidence suggest that the aromatic ring of Tyr-401 faces the central axis of the pore (23,46), and that a stable blocking site for Ca^{2+} is likely to be at the DEKA ring, where it can interact with the two acidic side chains (3). The structural model in Fig. 7, with calcium hexahydrate at a more superficial location near Tyr-401, is also likely to be nonconductive for Na^+ ions because of both the substantial volume occupied by the hydrated metal ion and its charge. Therefore, this conformation is also a blocked state, albeit weaker, presumably, than the site at the DEKA ring. We propose that the aromatic ring does not interact with this hydrated ion when it is in its deeper blocking site at the DEKA ring. Rather, the aromatic side chain affects the local concentration of Ca^{2+} ($[Ca^{2+}]_{local}$) in the immediate vicinity of this deeper site. Within the limits of reliability of the structural model in Fig. 7, a hydrated Ca^{2+} ion must pass near the aromatic face of Tyr-401 on its way to its deeper site at the DEKA ring. The probability of finding calcium hexahydrate at the location shown in the figure can be expressed as

$$p_j = \frac{1}{1+\exp\left(\Delta G_j/RT\right)},$$

where j is the number of fluorines, $\Delta G_j = \Delta G_{Phe_j} + \sum_k \Delta G_k$ is the free energy of calcium hexahydrate at that location, R is the universal gas constant, and T is the absolute temperature. ΔG_{Phe_j} is the contribution to the free energy of the aromatic ring, and $\sum_k \Delta G_k$ represents all other contributions due to the environment in the vicinity of the aromatic side chain. If we assume that in this aqueous environment p_j is very low, due both to the low dielectric walls of the vestibule and to the positive energy contributed by the aromatic ring (Fig. 6 *D*), then

$$p_j \simeq \exp\left(\frac{-\sum_k \Delta G_k}{RT}\right) \times \exp\left(\frac{-\Delta G_{Phe_j}}{RT}\right).$$

The $[Ca^{2+}]_{local}$ is proportional to p_j, leading to the prediction that the ratio of inhibition constants $K_j(0)/K_0(0) = p_0/p_j = \exp\left((\Delta G_{Phe_j} - \Delta G_{Phe_0})/RT\right) = \exp\left(\Delta\Delta G_j/RT\right)$. Because $\Delta\Delta G_j$ increases linearly with fluorination (Fig. 6 *D*), this exponential relationship conforms exactly with our experimental results (Fig. 5).

It remains for us to consider why the electrostatic effect of fluorinating the aromatic has little consequence on single-channel conductance. The primary reason, we propose, is that changes in electrostatic potential will have a larger effect on divalent Ca^{2+} ions than on the monovalent Na^+ ions that carry the inward current. Using the above quantum-mechanical approach for calculating the interaction energy of a Na^+ ion with benzene in water, we find, for example, that trifluorinating benzene has an approximately sixfold greater effect on $[Ca^{2+}]_{local}$ than on $[Na^+]_{local}$ at a distance of 4 Å from the center of the ring. Therefore the approximately threefold increase in $K_j(0)$ for Ca^{2+} block between Phe and 3,4,5F_3-Phe (Fig. 5) would correspond roughly to a 50% decrease in $[Na^+]_{local}$. This would have only a moderate effect on single-channel current amplitude, because $[Na^+]$ has a nonlinear, saturating relationship with single-channel conductance (6,14,47).

The above analysis sidestepped the explicit role of the conserved negatively charged ring (Fig. 1, *EEDD*) that will tend to concentrate cations within the extracellular vestibule. Functional studies suggest that the negative electrostatic potential in the vestibule is in excess of −100 mV (14,48). As we have seen here, however, a more challenging task for the channel is to overcome the energetic burden for metal cations to leave the relative comfort of the extracellular solution and enter a cavity lined by low-dielectric protein. Our calculations show that even in the presence of an

electrostatic potential of −140 mV at a distance of 5.7 Å from a benzene ring (Fig. 6 *A*), the aqueous environment remains unfavorable for Ca^{2+} (+15.3 kcal/mol) and only slightly favorable for Na^+ (−0.24 kcal/mol). Nevertheless, neutralizing any of the EEDD charges has substantial effects on both cation block and single-channel conductance (13,14,19,34,35), confirming a strong role for electrostatics.

The cation-π interaction has been examined extensively in the past two decades and is now known to play a significant energetic role in the interaction between organic cations and proteins, as well as between basic and aromatic side chains in proteins (45,49,50). A previous study, however, found no evidence for a postulated cation-π interaction between the divalent cation Mg^{2+} and the aromatic side chain of a Trp residue in a glutamate receptor (51). As we discussed here, this may not be surprising when the cation is very small and highly charged. One feature of a strong cation-π interaction is the match of hydration energies between a large cation, with its delocalized charge, and an aromatic ring. In the absence of other energetic constraints, the hydration mismatch between a Ca^{2+} ion and an aromatic ring precludes direct binding, despite a powerful electrostatic attraction. Nevertheless, we observe a systematic reduction of blocking affinity for Ca^{2+} as Phe-401 is progressively fluorinated, a distinguishing characteristic of a cation-π mechanism. Although induction (polarization) energy makes an attractive energetic contribution for both monovalent and divalent cations with benzene (52,53), the predominant consequences of fluorination arise from changes of the electrostatic interaction between the metal cation and the quadrupole moment of the aromatic ring (30,54). In comparison to the threefold destabilization of Ca^{2+} block, trifluorinating Phe-401 destabilizes the organic pore-blocker TTX, a monovalent cation, by 50-fold (23), suggesting a more intimate interaction between Phe-401 and the larger toxin in its binding site.

Although our study reveals a modest role for a cation-π mechanism in the interaction between a Ca^{2+} ion and an aromatic residue at position 401, it does not address isoform differences between TTX-sensitive channels that have an aromatic residue at this position and TTX-resistant channels that have either a Cys or a Ser at 401. Differences in Ca^{2+} block between these two classes of sodium channels is a disputed experimental observation (compare works by Weiss and Horn (21) and Chahine et al. (22) with studies by Ravindran et al. (10) and Sheets and Hanck (11)). This suggests that other factors might contribute to functional differences between these types of channels. It is also worth bearing in mind that fluorination of Phe-401 is a relatively minor perturbation of structure compared with mutating this residue into a Cys. Notably, only two amino acids distinguish the outer vestibule residues of $Na_V1.4$, the TTX-sensitive channel we study here, and the TTX-resistant cardiac channel $Na_V1.5$. The latter isoform has a Cys at the aligned position of Tyr-401, and an Arg instead of an Asn immediately adjacent to the outer ring of negative charge in D1. The Asn-to-Arg substitution of this residue by itself causes an ~10-fold decrease in Ca^{2+} block in a TTX-sensitive neuronal sodium channel (3), suggesting another electrostatic determinant of the local concentration of Ca^{2+} ions in the outer vestibule. The relative roles of these two residues will undoubtedly lead to insights into mechanisms of permeation and block in sodium channels.

In summary, our study demonstrates an electrostatic interaction between an aromatic side chain and Ca^{2+} ions within the outer mouth of a voltage-gated sodium channel. High-level quantum mechanical calculations show that the interaction is likely to occur between the hydrated cation and the aromatic ring.

We thank Mary Y. Ryan for help with oocytes and molecular biology.

This work was supported by grants from the National Institutes of Health (GM079427 and NS34407).

REFERENCES

1. Heinemann, S. H., H. Terlau, W. Stühmer, K. Imoto, and S. Numa. 1992. Calcium channel characteristics conferred on the sodium channel by single mutations. *Nature.* 356:441–443.
2. Favre, I., E. Moczydlowski, and L. Schild. 1996. On the structural basis for ionic selectivity among Na^+, K^+, and Ca^{2+} in the voltage-gated sodium channel. *Biophys. J.* 71:3110–3125.
3. Schlief, T., R. Schönherr, K. Imoto, and S. H. Heinemann. 1996. Pore properties of rat brain II sodium channels mutated in the selectivity filter domain. *Eur. Biophys. J.* 25:75–91.
4. Tsushima, R. G., R. A. Li, and P. H. Backx. 1997. Altered ionic selectivity of the sodium channel revealed by cysteine mutations within the pore. *J. Gen. Physiol.* 109:463–475.
5. Sun, Y. M., I. Favre, L. Schild, and E. Moczydlowski. 1997. On the structural basis for size-selective permeation of organic cations through the voltage-gated sodium channel. Effect of alanine mutations at the DEKA locus on selectivity, inhibition by Ca^{2+} and H^+, and molecular sieving. *J. Gen. Physiol.* 110:693–715.
6. Yamamoto, D., J. Z. Yeh, and T. Narahashi. 1984. Voltage-dependent calcium block of normal and tetramethrin-modified single sodium currents. *Biophys. J.* 45:337–344.
7. Sheets, M. F., B. E. Scanley, D. A. Hanck, J. C. Makielski, and H. A. Fozzard. 1987. Open sodium channel properties of single canine cardiac Purkinje cells. *Biophys. J.* 52:13–22.
8. Nilius, B. 1988. Calcium block of guinea-pig heart sodium channels with and without modification by the piperazinylindole DPI 201-106. *J. Physiol.* 399:537–558.
9. Behrens, M. I., A. Oberhauser, F. Bezanilla, and R. Latorre. 1989. Batrachotoxin-modified sodium channels from squid optic nerve in planar bilayers. Ion conduction and gating properties. *J. Gen. Physiol.* 93:23–41.
10. Ravindran, A., L. Schild, and E. Moczydlowski. 1991. Divalent cation selectivity for external block of voltage-dependent Na^+ channels prolonged by batrachotoxin. Zn^{2+} induces discrete substates in cardiac Na^+ channels. *J. Gen. Physiol.* 97:89–115.
11. Sheets, M. F., and D. A. Hanck. 1992. Mechanisms of extracellular divalent and trivalent cation block of the sodium current in canine cardiac Purkinje cells. *J. Physiol.* 454:299–320.
12. Hille, B. 2001. Ion Channels of Excitable Membranes. Sinauer Associates, Sunderland, MA.
13. Terlau, H., S. H. Heinemann, W. Stühmer, M. Pusch, F. Conti, K. Imoto, and S. Numa. 1991. Mapping the site of block by tetrodotoxin and saxitoxin of sodium channel II. *FEBS Lett.* 293:93–96.

14. Chiamvimonvat, N., M. T. Pérez-García, G. F. Tomaselli, and E. Marban. 1996. Control of ion flux and selectivity by negatively charged residues in the outer mouth of rat sodium channels. *J. Physiol.* 491:51–59.
15. Khan, A., J. W. Kyle, D. A. Hanck, G. M. Lipkind, and H. A. Fozzard. 2006. Isoform-dependent interaction of voltage-gated sodium channels with protons. *J. Physiol.* 576:493–501.
16. Backx, P. H., D. T. Yue, J. H. Lawrence, E. Marban, and G. F. Tomaselli. 1992. Molecular localization of an ion-binding site within the pore of mammalian sodium channels. *Science.* 257:248–251.
17. Chen, L.-Q., M. Chahine, R. G. Kallen, R. L. Barchi, and R. Horn. 1992. Chimeric study of sodium channels from rat skeletal and cardiac muscle. *FEBS Lett.* 309:253–257.
18. Satin, J., J. W. Kyle, M. Chen, P. Bell, L. L. Cribbs, H. A. Fozzard, and R. B. Rogart. 1992. A mutant of TTX-resistant cardiac sodium channels with TTX-sensitive properties. *Science.* 256:1202–1205.
19. Penzotti, J. L., H. A. Fozzard, G. M. Lipkind, and S. C. Dudley, Jr. 1998. Differences in saxitoxin and tetrodotoxin binding revealed by mutagenesis of the Na^+ channel outer vestibule. *Biophys. J.* 75:2647–2657.
20. Leffler, A., R. I. Herzog, S. D. Dib-Hajj, S. G. Waxman, and T. R. Cummins. 2005. Pharmacological properties of neuronal TTX-resistant sodium channels and the role of a critical serine pore residue. *Pflugers Arch.* 451:454–463.
21. Weiss, R. E., and R. Horn. 1986. Single-channel studies of TTX-sensitive and TTX-resistant sodium channels in developing rat muscle reveal different open channel properties. *Ann. N. Y. Acad. Sci.* 479: 152–161.
22. Chahine, M., L.-Q. Chen, R. G. Kallen, R. L. Barchi, and R. Horn. 1992. Expressed Na channel clones differ in their sensitivity to external calcium concentration. *Biophys. J.* 62:37–40.
23. Santarelli, V. P., A. L. Eastwood, D. A. Dougherty, R. Horn, and C. A. Ahern. 2007. A cation-π interaction discriminates among sodium channels that are either sensitive or resistant to tetrodotoxin block. *J. Biol. Chem.* 282:8044–8051.
24. Nowak, M. W., P. C. Kearney, J. R. Sampson, M. E. Saks, C. G. Labarca, S. K. Silverman, W. Zhong, J. Thorson, J. N. Abelson, N. Davidson, P. G. Schultz, D. A. Dougherty, and H. A. Lester. 1995. Nicotinic receptor binding site probed with unnatural amino acid incorporation in intact cells. *Science.* 268:439–442.
25. Ahern, C. A., A. L. Eastwood, H. A. Lester, D. A. Dougherty, and R. Horn. 2006. A cation-π interaction between extracellular TEA and an aromatic residue in potassium channels. *J. Gen. Physiol.* 128:649–657.
26. Cannon, S. C., A. I. McClatchey, and J. F. Gusella. 1993. Modification of the Na^+ current conducted by the rat skeletal muscle alpha subunit by coexpression with a human brain beta subunit. *Pflugers.* 423:155–157.
27. Narahashi, T. 1986. Modulators acting on sodium and calcium channels: patch-clamp analysis. *Adv. Neurol.* 44:211–224.
28. Marten, B., K. Kim, C. Cortis, R. A. Friesner, R. B. Murray, M. N. Ringnalda, D. Sitkoff, and B. Honig. 1996. New model for calculation of solvation free energies: correction of self-consistent reaction field continuum dielectric theory for short-range hydrogen-bonding effects. *J. Phys. Chem.* 100:11775–11788.
29. Williams, J. H. 1993. The molecular electric quadrupole moment and solid-state architecture. *Accounts Chem. Res.* 26:593–598.
30. Mecozzi, S., A. P. West, Jr., and D. A. Dougherty. 1996. Cation-π interactions in simple aromatics: electrostatics provide a predictive tool. *J. Am. Chem. Soc.* 118:2307–2308.
31. Woodhull, A. M. 1973. Ionic blockage of sodium channels in nerve. *J. Gen. Physiol.* 61:687–708.
32. Sansom, M. S., G. R. Smith, C. Adcock, and P. C. Biggin. 1997. The dielectric properties of water within model transbilayer pores. *Biophys. J.* 73:2404–2415.
33. Islas, L. D., and F. J. Sigworth. 2001. Electrostatics and the gating pore of *Shaker* potassium channels. *J. Gen. Physiol.* 117:69–89.
34. Noda, M., H. Suzuki, S. Numa, and W. Stühmer. 1989. A single point mutation confers tetrodotoxin and saxitoxin insensitivity on the sodium channel II. *FEBS Lett.* 259:213–216.
35. Chiamvimonvat, N., M. T. Pérez-García, R. Ranjan, E. Marban, and G. F. Tomaselli. 1996. Depth asymmetries of the pore-lining segments of the Na^+ channel revealed by cysteine mutagenesis. *Neuron.* 16:1037–1047.
36. Pérez-García, M. T., N. Chiamvimonvat, E. Marban, and G. F. Tomaselli. 1996. Structure of the sodium channel pore revealed by serial cysteine mutagenesis. *Proc. Natl. Acad. Sci. USA.* 93:300–304.
37. Chen, S. F., H. A. Hartmann, and G. E. Kirsch. 1997. Cysteine mapping in the ion selectivity and toxin binding region of the cardiac Na^+ channel pore. *J. Membr. Biol.* 155:11–25.
38. Vrbancich, J., and G. L. D. Ritchie. 1980. Quadrupole moments of benzene, hexafluorobenzene and other non-dipolar aromatic molecules. *J. Chem. Soc., Faraday Trans. 2.* 76:648–659.
39. Gallivan, J. P., and D. A. Dougherty. 2000. A computational study of cation-π interactions versus salt bridges in aqueous media: implications for protein engineering. *J. Am. Chem. Soc.* 122:870–874.
40. Bakó, I., J. Hutter, and G. Pálinkás. 2002. Car-Parrinello molecular dynamics simulation of the hydrated calcium ion. *J. Chem. Phys.* 117:9838–9843.
41. Asthagiri, D., L. R. Pratt, M. E. Paulaitis, and S. B. Rempe. 2004. Hydration structure and free energy of biomolecularly specific aqueous dications, including Zn^{2+} and first transition row metals. *J. Am. Chem. Soc.* 126:1285–1289.
42. McFail-Isom, L., X. Shui, and L. D. Williams. 1998. Divalent cations stabilize unstacked conformations of DNA and RNA by interacting with base π systems. *Biochemistry.* 37:17105–17111.
43. Zaric, S. D., D. M. Popovic, and E. W. Knapp. 2000. Metal ligand aromatic cation-π interactions in metalloproteins: ligands coordinated to metal interact with aromatic residues. *Chemistry (Easton).* 6:3935–3942.
44. Kumpf, R. A., and D. A. Dougherty. 1993. A mechanism for ion selectivity in potassium channels: computational studies of cation-π interactions. *Science.* 261:1708–1710.
45. Chipot, C., B. Maigret, D. A. Pearlman, and P. A. Kollman. 1996. Molecular dynamics potential of mean force calculations: a study of toluene-ammonium π-cation interactions. *J. Am. Chem. Soc.* 118: 2998–3005.
46. Lipkind, G. M., and H. A. Fozzard. 2005. Molecular modeling of local anesthetic drug binding by voltage-gated Na channels. *Molec Pharmac.* 68:1611–1622.
47. Begenisich, T. B., and M. D. Cahalan. 1980. Sodium channel permeation in squid axons. II: Non-independence and current-voltage relations. *J. Physiol.* 307:243–257.
48. Hui, K., D. McIntyre, and R. J. French. 2003. Conotoxins as sensors of local pH and electrostatic potential in the outer vestibule of the sodium channel. *J. Gen. Physiol.* 122:63–79.
49. Ma, J. C., and D. A. Dougherty. 1997. The cation-π interaction. *Chem. Rev.* 97:1303–1324.
50. Gallivan, J. P., and D. A. Dougherty. 1999. Cation-π interactions in structural biology. *Proc. Natl. Acad. Sci. USA.* 96:9459–9464.
51. McMenimen, K. A., D. A. Dougherty, H. A. Lester, and E. J. Petersson. 2006. Probing the Mg^{2+} blockade site of an N-methyl-D-aspartate (NMDA) receptor with unnatural amino acid mutagenesis. *ACS Chem Biol.* 1:227–234.
52. Cubero, E., F. J. Luque, and M. Orozco. 1998. Is polarization important in cation-π interactions? *Proc. Natl. Acad. Sci. USA.* 95: 5976–5980.
53. Tsuzuki, S., T. Uchimaru, and M. Mikami. 2003. Is the cation/π interaction in alkaline-earth-metal dication/benzene complexes a covalent interaction? *J. Phys. Chem. A.* 107:10414–10418.
54. Mecozzi, S., A. P. West, Jr., and D. A. Dougherty. 1996. Cation-π interactions in aromatics of biological and medicinal interest: electrostatic potential surfaces as a useful qualitative guide. *Proc. Natl. Acad. Sci. USA.* 93:10566–10571.